WARWICK
THE UNIVERSITY OF WARWICK

Original citation:
Maddar, Faduma, Lazenby, Robert A., Patel, Anisha N. and Unwin, Patrick R.. (2016) Electrochemical oxidation of dihydronicotinamide adenine dinucleotide (NADH) : Comparison of highly oriented pyrolytic graphite (HOPG) and polycrystalline boron-doped diamond (pBDD) electrodes. Physical Chemistry Chemical Physics.

Permanent WRAP URL:
http://wrap.warwick.ac.uk/81637

Copyright and reuse:
The Warwick Research Archive Portal (WRAP) makes this work of researchers of the University of Warwick available open access under the following conditions. Copyright © and all moral rights to the version of the paper presented here belong to the individual author(s) and/or other copyright owners. To the extent reasonable and practicable the material made available in WRAP has been checked for eligibility before being made available.

Copies of full items can be used for personal research or study, educational, or not-for-profit purposes without prior permission or charge. Provided that the authors, title and full bibliographic details are credited, a hyperlink and/or URL is given for the original metadata page and the content is not changed in any way.

Publisher statement:
First published by Royal Society of Chemistry 2016
http://dx.doi.org/10.1039/C6CP05394G
A note on versions:
The version presented here may differ from the published version or, version of record, if you wish to cite this item you are advised to consult the publisher's version. Please see the 'permanent WRAP URL' above for details on accessing the published version and note that access may require a subscription.

For more information, please contact the WRAP Team at: wrap@warwick.ac.uk

ARTICLE

Electrochemical oxidation of dihydronicotinamide adenine dinucleotide (NADH): Comparison of highly oriented pyrolytic graphite (HOPG) and polycrystalline boron-doped diamond (pBDD) electrodes
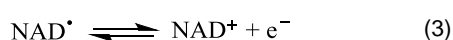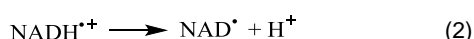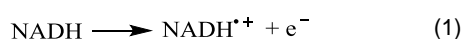
Faduma M. Maddar,[a] Robert A. Lazenby,[a] Anisha N. Patel [a,b] and Patrick R. Unwin*[a]

The electro-oxidation of nicotinamide adenine dinucleotide (NADH) is studied at bare surfaces of highly oriented pyrolytic graphite (HOPG) and semi-metallic polycrystalline boron-doped diamond (pBDD). A comparison of these two carbon electrode materials is interesting because they possess broadly similar densities of electronic states that are much lower than most metal electrodes, but graphite has carbon sp^2-hybridization, while in diamond the carbon is sp^3-hybridised, with resulting major differences in bulk structure and surface termination. Using cyclic voltammetry (CV), it is shown that NADH oxidation is facile at HOPG surfaces but the reaction products tend to strongly adsorb, which causes rapid deactivation of the electrode activity. This is an important factor that needs to be taken into account when assessing HOPG and its intrinsic activity. It is also shown that NADH itself adsorbs at HOPG, a fact that has not been recognized previously, but has implications for understanding the mechanism of the electro-oxidation process. Although pBDD was found to be less susceptible to surface fouling, pBDD is not immune to deterioration of the electrode response, and the reaction showed more sluggish kinetics on this electrode. Scanning electrochemical cell microscopy (SECCM) highlights a significant voltammetric variation in electroactivity between different crystal surface facets that are presented to solution with a pBDD electrode. The electroactivity of different grains correlates with the local dopant level, as visualized by field emission-scanning electron microscopy. SECCM measurements further prove that the basal plane of HOPG has high activity towards NADH electro-oxidation. These new insights on NADH voltammetry are useful for the design of optimal carbon-based electrodes for NADH electroanalysis.

Introduction

Nicotinamide adenine dinucleotide (NADH) is an essential co-factor in various naturally occurring enzymatic reactions such as the oxidation of ethanol catalyzed by the enzyme alcohol dehydrogenase.[1] NADH is the terminal electron donor in the mitochondrial electron transport chain. As such, the development of robust methods of analysis for NADH is of considerable importance, with electrochemical methods proving particularly effective. The mechanism of NADH oxidation has been studied extensively by Moiroux and Elving[2-5] and it is well established that at neutral pH, NADH undergoes a two-electron one-proton oxidation process of the ECE (electron transfer-chemical step-electron transfer) type:

$$NADH \longrightarrow NADH^{•+} + e^- \qquad (1)$$

$$NADH^{•+} \longrightarrow NAD^{•} + H^+ \qquad (2)$$

$$NAD^{•} \rightleftharpoons NAD^+ + e^- \qquad (3)$$

A wide range of carbon electrode materials have received considerable attention for NADH electro-oxidation, including glassy carbon,[4,6] carbon paste,[7] carbon nanotubes,[8,9] graphene[10] and graphene composites,[11-13] pyrolytic graphite[14] and boron-doped diamond.[15] The study of NADH oxidation on bare carbon electrode surfaces is non-trivial.[16] Relatively high overpotentials are often required and, furthermore, the oxidation products of NADH, particularly NAD^+ tend to adsorb strongly and foul surfaces quickly.[5,17,18]

Electrode surface modification has been considered as a means of achieving an effective decrease in overpotential for NADH oxidation.[19,20] However, studies of unmodified electrodes are valuable both to provide a benchmark and to seek the optimal electrode format. The electrochemistry of NADH at conducting diamond has received attention, but the focus has mainly been on hydrogen-terminated diamond,[15,21] with oxygen terminated diamond[14] receiving only scant attention. Despite its importance as a well-defined model surface for sp^2 carbon, there are no reports of NADH oxidation at highly oriented pyrolytic graphite (HOPG) electrodes. It is

a. Department of Chemistry, University of Warwick, Coventry, CV4 7AL, U.K.
b. Interfaces, Traitements, Organisation et Dynamique des Systèmes Laboratory, Sorbonne Paris Cité, Paris Diderot University, CNRS-UMR 7086, 15 rue J. A. Baif, 75013 Paris, France.
E-mail: p.r.unwin@warwick.ac.uk

important to note that the oxidation of NADH has been investigated at edge plane pyrolytic graphite (EPPG) and basal plane pyrolytic graphite (BPPG),[14] but these materials should not be confused with HOPG. BPPG is a material with a much smaller crystallite size than HOPG, and hence has considerable edge plane character similar, in fact, to EPPG.[22]

Comparison of electrochemical processes at HOPG and pBDD electrodes is interesting as they have broadly similar densities of electronic states (DOS) at the Fermi level over the typical range of potentials relevant for electrochemistry $ca.$ (2−6) × 10^{20} cm^{-3} eV^{-1},[23,24] that is about 1-2 orders of magnitude lower than metal electrodes. Yet, in other respects these materials may show different properties from each other. pBDD is sp^3 hybridized and compared to other carbon electrodes, shows relatively high immunity to deactivation via fouling, long term stability and excellent reproducibility of voltammetry for many electrode reactions and repetitive voltammetric cycling.[25] HOPG is an sp^2 carbon, the surface of which can readily be prepared and renewed via mechanical cleavage. It comprises of extensive basal terraces with a low density of point defects,[26,27] and a step edge density that depends on the grade (quality) of the HOPG.[28,29] Although early work considered the basal surface of HOPG to have ultra-low (or no) electrochemical activity,[27,29-39] recent studies have highlighted the high activity of the basal surface for both simple redox reactions and more complex coupled electron-proton transfer processes.[22,40,41] In the case of outer sphere redox processes, electron transfer rates are at least as fast at HOPG as on platinum.[27]

The studies reported herein on the electrochemical oxidation of NADH at HOPG and oxygen-terminated pBDD reinforce, and amplify, the recent models on the properties and activity of these electrode materials, while also providing detailed new insights on adsorption and surface fouling (contamination) processes. These measurements are complemented with high resolution scanning electrochemical cell microscopy (SECCM) [42,43] experiments to map the electrochemical activity of HOPG and pBDD and confirm the macroscopic findings. We make extensive use of macroscopic measurements at well-defined surfaces, for example, comparing the intrinsic activity of three different grades of HOPG that span step-edge density of more than 2 orders of magnitude.[29,41]

Experimental section

Materials and solutions

All chemicals were used as received. Aqueous solutions were prepared using high purity water (Purite, Select HP) with a resistivity of 18.2 MΩ cm at 25 °C. β-Nicotinamide adenine dinucleotide, reduced dipotassium salt hydrate (NADH, > 98 %), and phosphate buffer solution (pH 7.2) were purchased from Sigma-Aldrich. Sodium chloride (NaCl, 99.0 %, Sigma-Aldrich) was added to the phosphate buffer to give a phosphate buffer saline (PBS) solution. The working electrodes

used in this study were a highly doped pBDD electrode, and HOPG electrodes of varying step edge density. A 1 mm diameter pBDD disk electrode, used for macroscale electrochemistry was prepared in house from DIAFILM EA grade material (Element Six Ltd.).[26,54] The average boron doping level of the pBDD material was $ca.$ 5 × 10^{20} atoms cm^{-3}, above the metallic threshold as confirmed by secondary ion mass spectrometry (SIMS).[53] The pBDD had a roughness of 1-2 nm within a facet and 1-5 nm between grains, flat on the scale of SECCM and voltammetric measurements.[51] Studies of basal plane HOPG employed one of three different grades: either ZYB or SPI-3 grade (SPI Supplies, West Chester, PA), or an ungraded HOPG sample of the highest quality,[30] originating from Dr. Arthur Moore at Union Carbide (now GE Advanced Ceramics), and kindly provided by Prof. R. L. McCreery of the University of Alberta, Canada, which we refer to throughout as "AM grade"). All HOPG samples were cleaved with Scotch tape to remove surface layers and reveal a fresh surface for study. This procedure has been shown to produce a very similar surface to mechanical cleavage.[30]

Macroscale electrochemistry

Cyclic voltammetry (CV) was carried out in a three-electrode setup using a potentiostat (CH Instruments Model 750A, Austin, TX). A silver chloride coated Ag wire (Ag/AgCl) served as a quasi-reference electrode (QRE), while Pt gauze was used as the counter electrode. The Ag/AgCl QRE has a stable potential because AgCl has fast dissolution kinetics but is sparingly soluble.[44] All potentials are quoted against this QRE. The working electrodes (HOPG or pBDD) were as described above. On HOPG, a Teflon cell designed in house was used to provide a well-defined 3 mm diameter working cell; this has been described in detail elsewhere.[29] Because the BDD disk was encapsulated in glass, this could simply be immersed in solution, along with the other electrodes. Solutions contained different concentrations of NADH, as specified, in 0.1 M PBS. All solutions were prepared fresh on the day of the experiments and kept in the dark at all times when not in use. CV was performed at various potential scan rates (50, 100, 200, 400, 600 and 800 mV s^{-1}) for the electro-oxidation of NADH at potentials between 0.0 and 1.0 V. CV measurements were made either: (1) as a series of different scan rates on an HOPG sample that was freshly cleaved before the series or (2) on a freshly cleaved surface for each scan rate. We make it clear when each protocol was used. The well-known scotch tape method was used to cleave HOPG.[23,27-29,33,41,45-49] Similarly, the CV response of pBDD was measured either with or without polishing the electrode surface between each CV, and we again state when each method was used. The pBDD electrode was polished with alumina particles ($ca.$ 0.05 μm particle size, Micropolish, Buehler, Germany) on a deionized water saturated polishing pad (Microcloth, Buehler, Germany) and then rinsed with deionized water to ensure the compete removal of alumina particles.

Scanning electrochemical cell microscopy

High-resolution electrochemical imaging (SECCM) was performed on freshly cleaved HOPG (AM grade) and pBDD. The setup is shown schematically in Figure 1 and is described thoroughly elsewhere.[43] In brief, a tapered dual-channel borosilicate pipette, (with an opening of *ca.* 400 nm for experiments on HOPG and *ca.* 1 μm for experiments on pBDD) was filled with electrolyte solution. Since the laser pipette pulling procedure produces two probes of closely similar dimension, the sister probe to that used for imaging was characterized with field emission-scanning electron microscopy (FE-SEM), at 5 kV using a SUPRA 55 variable-pressure system (Zeiss). The probe used was filled with 1 mM NADH (for experiments on HOPG) and 0.5 mM NADH in 0.1 M PBS solution (for experiments on pBDD). A Ag/AgCl quasi-reference counter electrode (QRCE) was inserted in each channel. The SECCM instrument comprised of a high dynamics *z*-piezoelectric positioner (P-753.3CD LISA, Physik Instrumente), on which the pipette probe was mounted and an *xy*-piezoelectric stage (P-622.2CL PIHera, Physik Instrumente) for sample mounting. Instrument control and data acquisition was achieved using an FPGA card (PCIe-7852R) with a LabVIEW 2011 interface (LabVIEW 9.0, National Instruments). A video camera (PL-B776U, Pixelink) with a ×2 magnification lens (44 mm, InfiniStix, Edmund Optics) was used to aid tip-positioning.

A 200 mV bias, V_1, was applied between the two QRCEs, giving rise to an ion conductance current (i_{DC}) across the meniscus formed at the end of the pipette (see Figure 1). The tip was oscillated sinusoidally perpendicular to the surface, using the output generated by a lock-in amplifier, at a frequency of 260 Hz, with a 20 nm peak-to-peak amplitude for the tip used for measurements on HOPG and a 60 nm peak-to-peak amplitude for the tip used for pBDD measurements. The oscillation induced an alternating component of the ion conductance current (i_{AC}) across the meniscus, when the meniscus was in contact with the substrate, and this was used as a set-point for feedback, to maintain a constant tip-to-substrate separation during imaging.[43] The currents, i_{AC} and i_{DC}, were measured simultaneously along with the electrode surface current (i_{sub}).

The SECCM maps covered a 10 × 10 μm area of HOPG consisting of 32 line scans (16 forward and 16 reverse) at a tip scan rate of 0.3 μm s^{-1}. Each line comprised of 12957 pixels, each pixel representing a current value that was the average of 256 readings. These measurements were made at a fixed working electrode potential of 0.5 V (low driving force, *vide infra*). For pBDD, we employed voltammetric SECCM[50] in which the potential was swept between 0.0 and 0.8 V, at 300 mV s^{-1} in which the theta pipette probe was approached to the surface until meniscus contact was made, as sensed by a change in i_{AC}. At each pixel (point of meniscus contact) the working electrode potential was swept between 0.0 V to 0.8 V (vs. Ag/AgCl QRCE) and the current-voltage response was recorded. Hopping scans on pBDD were recorded (typically

with a resolution of 40 × 30 pixels) over an area of 60 × 45 μm and consisted of the following: a probe approach rate towards the surface of 0.3 μm s^{-1} to meniscus contact; potential sweep of 300 mV s^{-1} (potential swept between 0.0 and 0.8 V); 1.2 μm retraction distance at a rate of 5 μm s^{-1}, enough to break the meniscus contact and move to the next position at a scan rate of 1.2 μm s^{-1}. The distance between each hop (pixel) was chosen to be 1.5 μm, to avoid the overlap of adjacent probed areas.
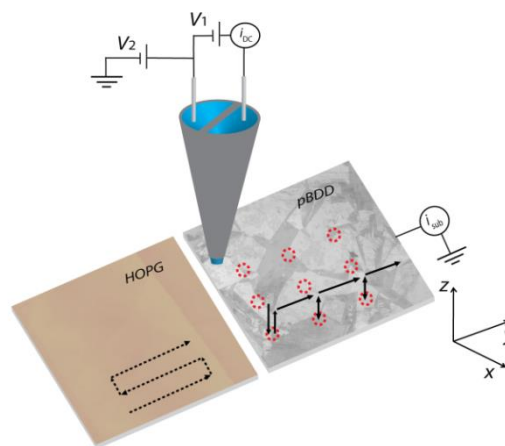

Figure 1. Schematic of the SECCM setup in which a theta pipette was used to create a tiny meniscus electrochemical cell on a carbon electrode surface (HOPG or pBDD) with the working electrode size determined by the size of the pipette opening and meniscus wetting of the substrate. An ion conductance current (i_{DC}) was generated by the potential bias, V$_1$, between the two barrels of the pipette, while the voltage, V$_2$, provided additional control of the potential of the working electrode. The resulting electrochemical current, i_{sub}, was measured to determine the local electroactivity. The conductance current has an AC component (see text for details), at the frequency of the pipette position modulation (z-direction).

AFM imaging

AFM images of HOPG topography were recorded in air, using an Innova® AFM in tapping mode (AM and SPI-3 HOPG) and a BioScope Catalyst™ BioAFM in ScanAsyst mode (ZYB HOPG).

Results and discussion

Voltammetry of NADH oxidation on HOPG and pBDD

We first consider macroscale cyclic voltammetry (CV) measurements as a function of scan rate for ZYB grade HOPG and pBDD. For the data in Figure 2 (a) and (b), where j represents current density, an initial CV was run on either a freshly cleaved graphite surface, or polished pBDD, respectively, with no subsequent cleaning or cleaving before the subsequent voltammetric sweeps. In order to determine whether there was any electrode surface blocking, or other systematic effects, from the electrochemical process, as alluded to in the introduction, the first sweep was run at 50 mV s^{-1}, followed by a set of subsequent sweeps at a series of increasingly faster scan rates (100, 200, 400, 600 and 800 mV s^{-1}). The first thing to note is the significant difference in the onset potential for the oxidation of NADH at the two different electrodes. On pBDD (Figure 2 (a)), the NADH oxidation peak occurred at a potential of $ca.$ +0.55 V (at 50 mV s^{-1}). As already noted, pBDD electrodes have high immunity to chemical fouling compared to other electrodes,[25] and so fairly well-defined successive waves are observed. The oxidation peak potential shifts slightly with increasing scan rate to a more positive potential. In comparison, in Figure 2 (b), at HOPG, electro-oxidation is much more facile, occurring at a lower anodic potential with a value of $ca.$ +0.40 V for the peak current (at 50 mV s^{-1}). However, for CVs at increasing scan rates, the peak current does not increase as much as might be expected, compared to the pBDD case, with the maximum peak current density being only $ca.$ 153 μA cm^{-2} at 800 mVs^{-1} ($cf.$ 596 μA cm^{-2} at 800 mV s^{-1} for pBDD). Moreover, it can be seen that with increasing scan rates (number of scans), the voltammetric response becomes complex, with additional features appearing at more anodic potentials. This behavior, and its comparison to the pBDD response and the behavior on a surface freshly prepared before each voltammagram (discussed below), is strongly indicative of the HOPG surface becoming blocked by NADH oxidation products, as found for other carbon electrode materials.[5,14]

For comparison, CVs were run, for the same scan rates, at freshly polished pBDD or freshly cleaved HOPG prior to each CV. The results, shown in Figure 2 (c) and (d), highlight similar voltammetric behavior at pBDD to the response in Figure 2 (a), in which the surface was not cleaned between each CV at each scan rate. For HOPG, the difference between Figure 2 (b) and Figure 2 (d) is stark. CVs on freshly cleaved surfaces showed well-defined peaks of much higher current density magnitude that scale reasonably with the square root of scan rate, as indicative of a diffusion-limited process. The positive shift in oxidation peak potential for the electrode process is mostly a consequence of the strong adsorption of NAD$^+$ that is produced at the electrode during the oxidation of NADH. Although NAD$^+$ may behave as a mediator of electron transfers from NADH to the electrode through the adsorbed layer, it inhibits the rate of the reaction.[2]
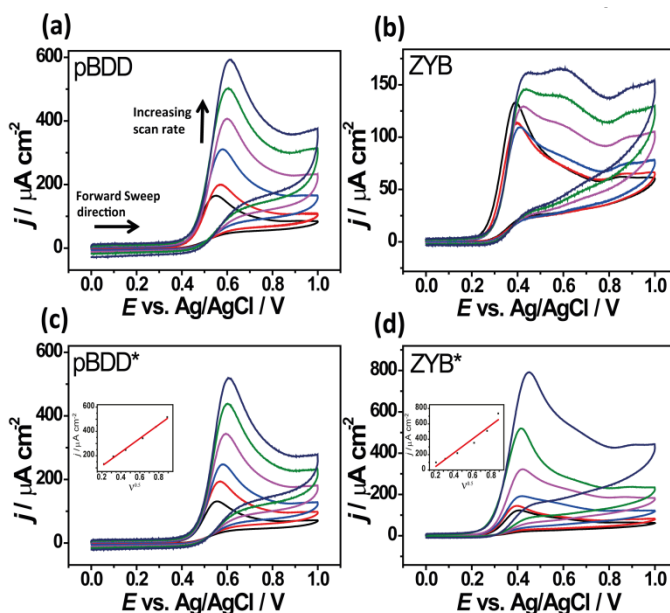

Figure 2. Oxidation of 1 mM NADH in 0.1 M PBS at various potential scan rates: 50, 100, 200, 400, 600 and 800 mV s^{-1}. For (a) pBDD and (b) ZYB the surface was cleaned or cleaved, respectively, prior to the first 50 mV s^{-1} scan, after which subsequent scans at increasing scan rates were run without further pretreatment or preparation of the electrode surface. For (c) pBDD* and (d) ZYB*, each voltammetric scan was made on a freshly polished pBDD or a freshly cleaved HOPG surface. The insets show plots of peak current vs. the square root of scan rate.

Repetitive cyclic voltammetric response

The extent to which the responses of the different carbon electrodes changed during NADH (1 mM) oxidation was studied by recording consecutive CVs (10 runs at 100 mV s^{-1}), with 5 s intervals between each CV, for each electrode. Figure 3 shows characteristic CVs for repetitive cycling using three grades of HOPG: (a) AM, (b) ZYB and (c) SPI-3, and (d) pBDD.

The behavior of the three different grades of HOPG is similar for the initial scan, even though the step edge densities vary by more than 2 orders of magnitude,[41] as shown in Figure 4. This strongly suggests that for graphite the electrochemical response is mainly determined by the basal surface, not the step edges. In the case of pBDD,[51-53] although recognized for combining high stability and resistance to chemical fouling, the repetitive cycling showed a decrease in current response over the 10 cycles, but not to the same extent as HOPG.
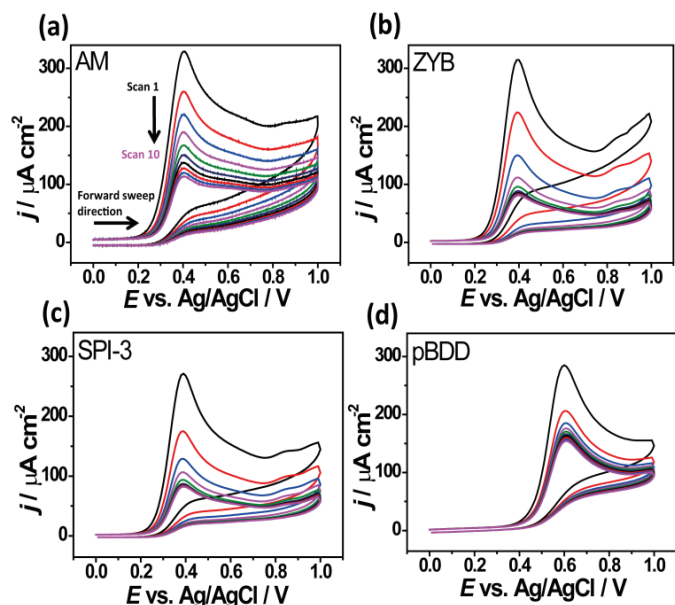
Figure 3. Repetitive CVs for the oxidation of 1 mM NADH on (a) AM, (b) ZYB, (c) SPI-3 grade HOPG and (d) pBDD in 0.1 M PBS, at a potential sweep rate of 100 mV s^{-1}. Each voltammogram was run with a 5 s interval between for a total of 10 cycles
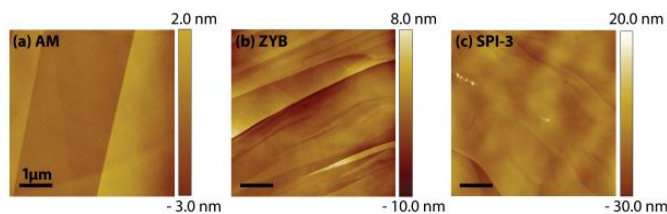

Figure 4. AFM topography images of freshly cleaved HOPG: (a) AM, (b) ZYB and (c) SPI-3 grades.

Adsorption behavior of NADH on HOPG

Although the studies herein indicate that the product of NADH adsorption, NAD$^+$, adsorbs on both HOPG and pBDD, in line with studies on other electrodes,[4,5] we sought to elucidate whether NADH adsorbed. Early work suggested that NADH does not adsorb on pyrolytic graphite electrodes, although measurements were made at mM levels of NADH in bulk solution, and low to moderate voltammetry scan rates,[4] where low levels of adsorption would be difficult to detect. For our studies we used HOPG, for which the background current is very low and decreased the concentration of NADH to 5 μM where the diffusional-electrochemical response would be greatly attenuated, compared to any signal for adsorbed material. CVs were run on freshly cleaved surfaces of AM, ZYB and SPI-3 HOPG at different scan rates (Figure 5 (a-c) (i)). Significant oxidative signals are seen that can be attributed to

adsorbed NADH, and the lack of any reverse process indicates that this is an irreversible (anodic stripping) process.[54] The data in Figure 5 (a-c) (ii) illustrate that the anodic peak current varies linearly with scan rate, as expected for electron-transfer to an adsorbed layer. Furthermore, the current density is noticeably greater on AM grade as compared to ZYB and SPI-3 HOPG. These latter grades of HOPG have higher step edge densities and we have found in some other cases,[27,28] that this appears to inhibit molecular adsorption. This suggests that the lateral interaction between adsorbed NADH is important, which is promoted on the extended basal surface of AM HOPG (Figure 4 (a)). This is also another explanation as to why NADH adsorption was not seen on pyrolytic graphite for which the step edge density is very high, along with the background (capacitive) currents during linear sweep voltammetry[22]

To quantify the amount of NADH adsorption, the area of the adsorbed voltammetric peaks was integrated to give the charge density, Q, for adsorbed NADH:

$$Q = nF\Gamma \qquad (4)$$

where $n = 2$ is the number of electrons involved in the redox reaction, and F is the Faraday constant, from which Γ, the surface concentration of NADH (mol cm^{-2}) could be obtained. Plots of charge density versus scan rate (v) for each HOPG grade are given in Figure 5 (a-c) (iii) from which we obtained Γ values of 2.05 x 10^{-11} mol cm^{-2} (AM grade), 1.03 x 10^{-11} mol cm^{-2} (ZYB) and 1.21 x 10^{-11} mol cm^{-2} (SPI-3). Thus, the adsorption extent is rather small, but detectable, due to the low background currents at HOPG.
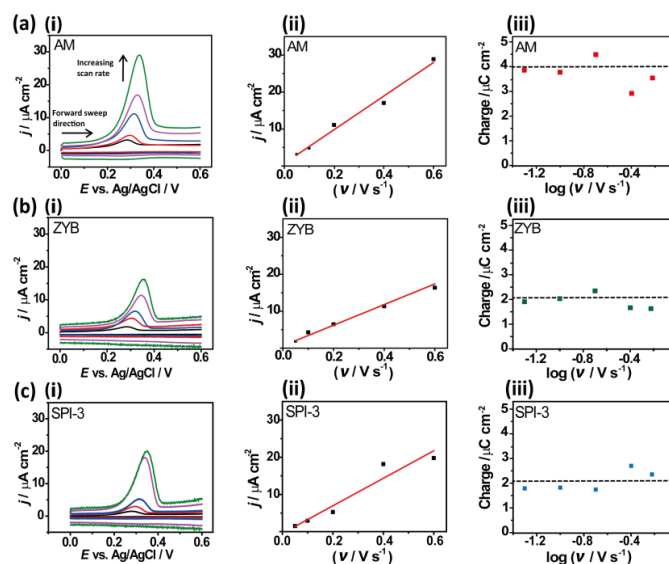

Figure 5. Oxidation of 5 μM NADH in 0.1 M PBS at various scan rates: 50, 100, 200, 400, and 600 mV s^{-1} at (a) (i) AM (b) (i) ZYB and (c) (i) SPI-3. (a-c) (ii) Plots of current density (forward wave) against scan rate and (a-c) (iii) variation of forward peak charge with the log of scan rate for the 3 different HOPG grades.

High resolution imaging of electrochemical activity

SECCM allows the measurement of surface electroactivity free from topographical effects.[55] As highlighted above, the process of NADH oxidation can lead to the rapid deterioration of the electrode surface activity, which means that conventional electrochemical imaging techniques, where the whole electrode surface would be immersed in solution and carrying out this reaction - as in the case for scanning electrochemical microscopy (SECM)[32] - would be of limited use. The advantage of SECCM is that only a small fraction of the surface at a time is in contact with the electrolyte solution during a scan. Moreover, by judicious selection of the local meniscus contact time, measurements can be made on a close to pristine surface, before surface blocking occurs, and blocking products can be left behind as the probe meniscus moves to a new location on the surface.[56]

We first consider HOPG (AM grade) measurements with the SECCM setup. Two successive CVs with 1 mM NADH on AM grade HOPG at 100 mV s^{-1} with a meniscus contact diameter of 400 nm are shown in Figure 6 (a). A large hysteresis between the forward and reverse waves is observed. On this CV time scale, which has a relatively high mass transfer coefficient, similar to a disk electrode of about 10 times the contact diameter (i.e. 4 μm),[57] a sigmoidal response would have been expected for a simple electrochemical reaction, with the forward and reverse waves closely similar.[58] The observation can be attributed to a blocking of the electrode. Additionally, the peak in the first forward wave decreases in the second scan, also indicating blocking of the electrode by reaction products. SECCM mapping of surface electrochemistry was carried out with 1 mM NADH in 0.1 M PBS at a potential of 0.5 V (Figure 6 (a)), in order to not fully drive the oxidation reaction and minimize blocking, with a lateral probe scan rate of 0.3 μm s^{-1}. The residence time was about 1 s and based on the measured currents of *ca.* 4 pA, about 10^7 molecules were turned over at the surface in contact with the meniscus cell. Figure 6 (b), the SECCM electrochemical activity map of HOPG, reveals fairly uniform activity across the surface, with current values similar to those in the initial values. Additonally, Figure 6 (c) shows uniform conductance current between the QRCEs in the barrels of the SECCM tip, indicating very stable mensicus contact and surface wetting, during imaging. From these maps we can readily conclude that the electrochemical reaction occurs easily at the basal surface of HOPG.

We now turn to the pBDD electrode. Figure 7 (a) (i) and (ii) shows an optical image of the SECCM probe and electrode before and after an image. Using the in-rig camera, the area where the image was made is marked by the deposition of product material. As mentioned in the experimental section, these measurements were run in a hopping –voltammetry mode (300 mV s^{-1}). This was possible because the extent of blocking of pBDD by NADH oxidation products is less extensive, although still occurs, as the positions where measurements were made were clearly revealed using FE-SEM by spot

deposits left behind (Figure 7 (a) (ii)). These spots are fairly consistent and approximate to the tip size (Figure 7 (a) (iv)). After cleaning the pBDD surface, we were able to visualize by FE-SEM the area in which an SECCM image was recorded. (Figure 7 (b) (i)).
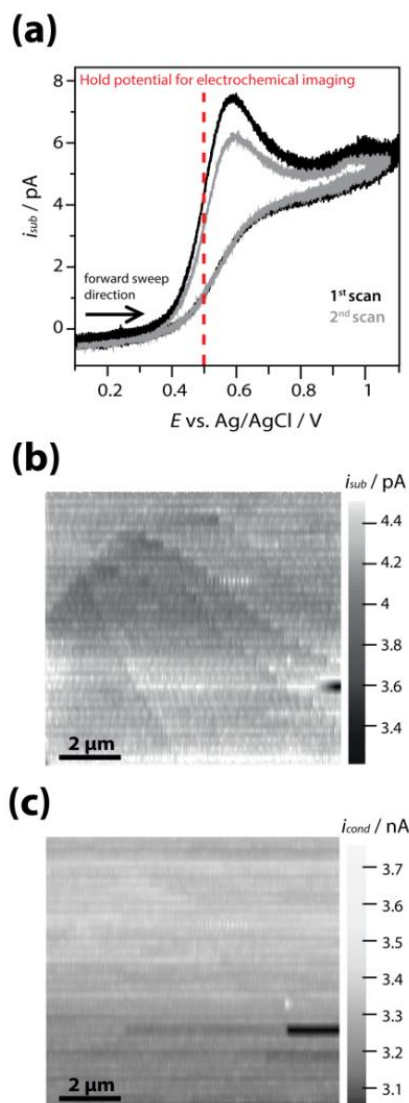

Figure 6. (a) SECCM CVs for the oxidation of 1 mM NADH in 0.1 M PBS at 100 mV s^{-1}. SECCM maps of (b) surface electrochemical activity and (c) conductance current (DC component) recorded at the half-wave potential for the oxidation of 1 mM NADH at HOPG (AM), obtained with a ca. 400 nm diameter pipette.

Previous FE-SEM studies confirmed that lighter and darker areas correspond to less-doped (more charging) and more-doped (less charging) facets respectively.[56,59] Potential-resolved snap shots of electrochemical activity, from a series of images, at potentials of 0.5 V, 0.6 V and 0.7 V are shown in Figure 7 (b) (ii-iv). Close to the onset of the oxidation current (0.5 V), we begin to see the appearance of the more-doped facets on the electrochemical image, and as the working

electrode potential is scanned positive, there is an increase in surface current, but particularly so in the more doped facets. Thus, for pBDD, the variation in the dopant level appear to have a significant impact on local electrochemical activity, as seen for a range of other reactions.[24,56] This needs to be taken into account to understand the electrochemical properties of this material and particularly in the analysis of macroscopic and voltammetric data.
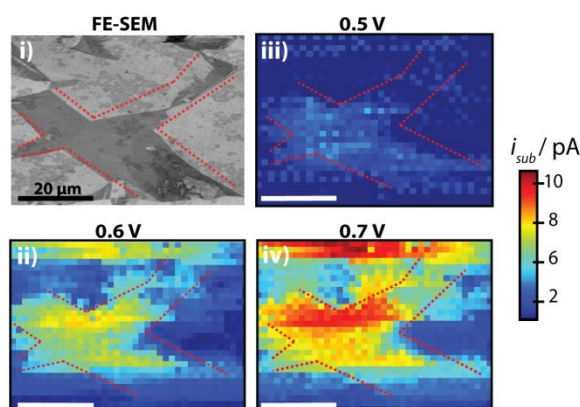
(a)
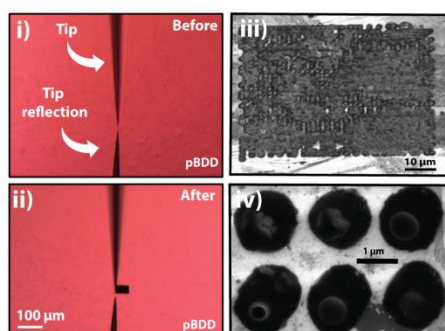
(b)

Figure 7. (a) (i) Optical microscope image of the pBDD substrate, taken using the in-rig camera before performing the SECCM map and (ii) after scan. (iii) FE-SEM micrograph of the scanned area, covered by spots of reaction products formed during each local voltammetric scan. (iv) FE-SEM micrograph showing a zoom of typical spots after hopping voltammetric mode SECCM imaging. (b) (i) FE-SEM image of the same area of pBDD after cleaning to remove the adsorbed material. (ii-iv) Snap shot SECCM electrochemical maps (60 μm × 45 μm) at different potentials, as marked above each map.

Conclusions

The voltammetric response of NADH at freshly cleaved HOPG and oxygen-terminated pBDD has been analyzed in detail at the macroscale using high-resolution electrochemical imaging. These two materials have relatively similar DOS, yet the electro-oxidation of NADH is much faster on the basal plane of HOPG than on pBDD. On the other hand, the electrochemical oxidation of NADH is a redox process complicated by side reactions. Oxidation products tend to adsorb onto the surface

and manifest in a deterioration of the electrochemical response, with this process occurring more extensively on HOPG than on pBDD. These effects need to be recognized and accounted for when considering the intrinsic behavior of these electrode materials.

The observations reported herein demonstrate that the electro-oxidation of NADH is facile at the basal plane of HOPG and independent of step edge density, as is the deterioration of the electrode response due to blocking by reaction products. The high intrinsic activity of the basal plane HOPG for these reactions has been demonstrated unequivocally using high resolution electrochemical imaging. An important new feature to NADH oxidation at sp^2 carbon electrodes revealed by this work is a contribution to the electrochemical response from adsorbed NADH, providing a further illustration of the potential importance of adsorbed reactants in electrochemistry at HOPG. The extent of adsorption (as inferred from the electrochemical signal) is enhanced at the highest quality (low step edge density) HOPG, i.e. is promoted by extensive basal surface regions.

For pBDD, electrochemical currents for NADH oxidation are strongly correlated with the local boron dopant concentration in individual facets. This is an important issue that must be taken into account in order to gain a holistic view of pBDD electrochemical characteristics.

References

1.   C. Lau, G.-U. Flechsig, P. Gründler and J. Wang, *Anal. Chim. Acta*, 2005, **554**, 74-78.
2.   J. Moiroux and P. J. Elving, *J. Am. Chem. Soc.*, 1980, **102**, 6533-6538.
3.   J. Moiroux and P. J. Elving, *Anal. Chem.*, 1979, **51**, 346-350.
4.   J. Moiroux and P. J. Elving, *J. Electroanal. Chem. Interfac.*, 1979, **102**, 93-108.
5.   J. Moiroux and P. J. Elving, *Anal.Chem.*, 1978, **50**, 1056-1062.
6.   M. Musameh, J. Wang, A. Merkoci and Y. Lin, *Electrochem. Commun.*, 2002, **4**, 743-746.
7.   L. Gorton, *Electroanalysis*, 1995, **7**, 23-45.
8.   M. Musameh, N. S. Lawrence and J. Wang, *Electrochem. Commun.*, 2005, **7**, 14-18.

9. M. Wooten and W. Gorski, *Anal. Chem.*, 2010, **82**, 1299-1304.

10. N. L. Ritzert, W. Li, C. Tan, G. G. Rodriguez-Calero, J. Rodriguez-Lopez, K. Hernandez-Burgos, S. Conte, J. J. Parks, D. C. Ralph and H. D. Abruna, *Faraday Discuss.*, 2014, **172**, 27-45.

11. K. R. Ratinac, W. Yang, J. J. Gooding, P. Thordarson and F. Braet, *Electroanalysis*, 2011, **23**, 803-826.

12. K. Chen, Z.-L. Zhang, Y.-M. Liang and W. Liu, *Sensors (Basel, Switzerland)*, 2013, **13**, 6204-6216.

13. W.-J. Lin, C.-S. Liao, J.-H. Jhang and Y.-C. Tsai, *Electrochem. Commun.*, 2009, **11**, 2153-2156.

14. C. E. Banks and R. G. Compton, *Analyst*, 2005, **130**, 1232-1239.

15. T. N. Rao, I. Yagi, T. Miwa, D. A. Tryk and A. Fujishima, *Anal. Chem.*, 1999, **71**, 2506-2511.

16. W. B. Nowall and W. G. Kuhr, *Anal. Chem.*, 1995, **67**, 3583-3588.

17. Z. Samec and P. J. Elving, *J. Electroanal. Chem. Interfac.*, 1983, **144**, 217-234.

18. W. J. Blaedel and R. A. Jenkins, *Anal. Chem.*, 1975, **47**, 1337-1343.

19. L. Gorton, *J. Chem. Soc., Faraday Trans. 1.*, 1986, **82**, 1245-1258.

20. L. Gorton and E. Domínguez, in *Encyclopedia of Electrochemistry*, Wiley-VCH Verlag GmbH & Co. KGaA, 2007, DOI: 10.1002/9783527610426.bard090004.

21. A. Fujishima, T. N. Rao, E. Popa, B. V. Sarada, I. Yagi and D. A. Tryk, *J. Electroanal. Chem.*, 1999, **473**, 179-185.

22. A. N. Patel, S.-y. Tan, T. S. Miller, J. V. Macpherson and P. R. Unwin, *Anal. Chem.*, 2013, **85**, 11755-11764.

23. K. R. Kneten and R. L. McCreery, *Anal. Chem.*, 1992, **64**, 2518-2524.

24. H. V. Patten, K. E. Meadows, L. A. Hutton, J. G. Iacobini, D. Battistel, K. McKelvey, A. W. Colburn, M. E. Newton, J. V. Macpherson and P. R. Unwin, *Angew. Chem. Int. Ed.*, 2012, **51**, 7002-7006.

25. L. A. Hutton, J. G. Iacobini, E. Bitziou, R. B. Channon, M. E. Newton and J. V. Macpherson, *Anal. Chem.*, 2013, **85**, 7230-7240.

26. H. Chang and A. J. Bard, *J. Am. Chem. Soc.*, 1991, **113**, 5588-5596.

27. G. Zhang, A. S. Cuharuc, A. G. Güell and P. R. Unwin, *Phys. Chem. Chem. Phys.*, 2015, **17**, 11827-11838.

28. G. Zhang, P. M. Kirkman, A. N. Patel, A. S. Cuharuc, K. McKelvey and P. R. Unwin, *J. Am. Chem. Soc.*, 2014, **136**, 11444-11451.

29. A. N. Patel, M. G. Collignon, M. A. O'Connell, W. O. Y. Hung, K. McKelvey, J. V. Macpherson and P. R. Unwin, *J. Am. Chem. Soc.*, 2012, **134**, 20117-20130.

30. T. J. Davies, R. R. Moore, C. E. Banks and R. G. Compton, *J. Electroanal. Chem.*, 2004, **574**, 123-152.

31. M. T. McDermott and R. L. McCreery, *Langmuir*, 1994, **10**, 4307-4314.

32. R. Bowler, T. J. Davies, M. E. Hyde and R. G. Compton, *Anal. Chem.*, 2005, **77**, 1916-1919.

33. S. C. S. Lai, A. N. Patel, K. McKelvey and P. R. Unwin, *Angew. Chem. Int. Ed.*, 2012, **51**, 5405-5408.

34. A. G. Güell, A. S. Cuharuc, Y.-R. Kim, G. Zhang, S.-y. Tan, N. Ebejer and P. R. Unwin, *ACS Nano*, 2015, **9**, 3558-3571.

35. S.-y. Tan, J. Zhang, A. M. Bond, J. V. Macpherson and P. R. Unwin, *Anal. Chem.*, 2016, **88**, 3272-3280.

36. A. S. Cuharuc, G. Zhang and P. R. Unwin, *Phys. Chem. Chem. Phys.*, 2016, **18**, 4966-4977.

37. P. L. Frederix, P. D. Bosshart, T. Akiyama, M. Chami, M. R. Gullo, J. J. Blackstock, K. Dooleweerdt, N. F. de Rooij, U. Staufer and A. Engel, *Nanotechnology*, 2008, **19**, 384004.

38. Y.-R. Kim, S. C. S. Lai, K. McKelvey, G. Zhang, D. Perry, T. S. Miller and P. R. Unwin, *J. Phys. Chem. C*, 2015, **119**, 17389-17397.

39. S. C. S. Lai, R. A. Lazenby, P. M. Kirkman and P. R. Unwin, *Chem. Sci.*, 2015, **6**, 1126-1138.

40. A. N. Patel, K. McKelvey and P. R. Unwin, *J. Am. Chem. Soc.*, 2012, **134**, 20246-20249.

41. A. N. Patel, S.-y. Tan and P. R. Unwin, *Chem. Commun.*, 2013, **49**, 8776-8778.

42. M. E. Snowden, A. G. Güell, S. C. S. Lai, K. McKelvey, N. Ebejer, M. A. O'Connell, A. W. Colburn and P. R. Unwin, *Anal. Chem.*, 2012, **84**, 2483-2491.

43. N. Ebejer, M. Schnippering, A. W. Colburn, M. A. Edwards and P. R. Unwin, *Anal. Chem.*, 2010, **82**, 9141-9145.

44. J. V. Macpherson and P. R. Unwin, *J. Phys. Chem.*, 1994, **98**, 1704-1713.

45. R. J. Rice and R. L. McCreery, *Anal. Chem.*, 1989, **61**, 1637-1641.

46. M. T. McDermott, K. Kneten and R. L. McCreery, *J. Phys. Chem.*, 1992, **96**, 3124-3130.

47. R. J. Bowling, R. T. Packard and R. L. McCreery, *J. Am. Chem. Soc.*, 1989, **111**, 1217-1223.

48. M. A. Edwards, P. Bertoncello and P. R. Unwin, *J. Phys. Chem. C*, 2009, **113**, 9218-9223.

49. M. Pumera, *Chem. Soc. Rev.*, 2010, **39**, 4146-4157.

50. C.-H. Chen, L. Jacobse, K. McKelvey, S. C. S. Lai, M. T. M. Koper and P. R. Unwin, *Anal. Chem.*, 2015, **87**, 5782-5789.

51. R. G. Compton, J. S. Foord and F. Marken, *Electroanalysis*, 2003, **15**, 1349-1363.

52. A. Kraft, *Int. J. Electrochem. Sci*, 2007, **2**, 355-385.

53. J. H. Luong, K. B. Male and J. D. Glennon, *Analyst*, 2009, **134**, 1965-1979.

54. A. J. Bard, L. R. Faulkner, *Electrochemical Methods: Fundamentals and Applications*, John Wiley & Sons, Inc. 2001. 589-608

55. N. Ebejer, A. G. Güell, S. C. S. Lai, K. McKelvey, M. E. Snowden and P. R. Unwin, *Annu. Rev. Anal. Chem. (Palo Alto Calif)*, 2013, **6**, 329-351.

56. H. V. Patten, S. C. S. Lai, J. V. Macpherson and P. R. Unwin, *Anal. Chem.*, 2012, **84**, 5427-5432.

57. C. G. Williams, M. A. Edwards, A. L. Colley, J. V. Macpherson and P. R. Unwin, *Anal. Chem.*, 2009, **81**, 2486-2495.

58. C. E. Banks, T. J. Davies, G. G. Wildgoose and R. G. Compton, *Chem. Commun.*, 2005, DOI: 10.1039/B413177K, 829-841.

59. N. R. Wilson, S. L. Clewes, M. E. Newton, P. R. Unwin and J. V. Macpherson, *J. Phys. Chem. B*, 2006, **110**, 5639-5646.